Agenzia nazionale per le nuove tecnologie,
l'energia e lo sviluppo economico sostenibile

MINISTERO DELLO SVILUPPO ECONOMICO

Ricerca di Sistema elettrico

Large Eddy Simulation (LES) di un Bruciatore Swirlato Metano/Aria

D. Cecere, E. Giacomazzi, F.R. Picchia, N. Arcidiacono

Report RdS/PAR2013/271

LARGE EDDY SIMULATION (LES) DI UN BRUCIATORE SWIRLATO METANO/ARIA

D. Cecere, E. Giacomazzi, F.R. Picchia, N. Arcidiacono, (ENEA, UTTEI-COMSO)

Settembre 2014

Report Ricerca di Sistema Elettrico
Accordo di Programma Ministero dello Sviluppo Economico – ENEA
Piano Annuale di Realizzazione 2013
Area: Produzione di energia elettrica e protezione dell'ambiente
Progetto: B.2 - Cattura e sequestro della CO2 prodotta dall'utilizzo di combustibili fossili
Obiettivo: Parte A - b - Tecnologie per l'ottimizzazione dei processi di combustione
Task b.1 - Metodologie numeriche avanzate per la simulazione dei processi di combustione e la progettazione di componenti
Responsabile del Progetto: Stefano Giammartini, ENEA

Indice

Sommario

In questo lavoro una simulazione LES é stata applicata all'analisi di un bruciatore swirlato con una miscela metano-aria magra. La complessa geometria del combustore é stata trattata nel codice comprimibile dell' ENEA HEART mediante la nuova tecnica Immersed Volume (IVM) sviluppata in ENEA. É stata adottata una griglia cartesiana strutturata di 55 milioni di nodi assieme ad uno schema cinetico dettagliato per la chimica del metano-aria costituita da 17 specie e 73 reazioni elementari. In questo lavoro vengono descritte le caratteristiche generali della fiamma all'interno del bruciatore. Il campo fluidodinamico all' interno della camera di combustione diviso in tre zone distinte: la zona di ingresso dei gas miscelati in camera di combustione, una zona di ricircolo interna intorno all'asse del combustore ed una esterna contigua alle pareti. La fiamma é ancorata all'uscita del bruciatore intorno a 0.035 m nella zona di ricircolo interna. Un significativo livello di non mescolamento é stato rilevato all'uscita del mozzo conico. Questo risultato, anche se parziale, suggerisce che alcuni fenomeni di instabilit termoacustici possano essere intensificati nella fiamma a causa del livello di non perfetta miscelazione. La simulazione é molto onerosa dal punto di vista computazionale, il passo di avanzamento temporale legato alla stabilit numerica degli schemi adottati é di 22 ns. Il calcolo é ancora in atto con lo scopo di simulare un tempo totale di alcuni centesimi di secondo in modo da poter includere nelle statistiche gli effetti delle fluttuazioni di pressione a bassa frequenza (290 Hz).

1 Introduction

In stationary gas turbines (GT) the concept of lean premixed combustion is widely used in order to meet the stringent demands for low emissions of NO_x . This concept also allows the achievement of a quite homogeneous temperature distribution at the turbine inlet and thus a lower thermal load. Unfortunately, lean premixed GT flames are susceptible to thermoacoustic instabilities driven by the combustion process and sustained by a resonant feedback mechanism coupling pressure and heat release. These pulsations can lead to strong perturbations in the gas turbine and even to the destruction of system components. The physical and chemical mechanisms driving the instabilities are based on a complex interaction between combustor geometry, pressure, flow fleld, mixing, chemical reactions, and heat release and are not understood well enough yet. Major efforts are currently being made in the development of numerical simulation tools in order to predict unsteady combustion behavior so that improved GT combustors can be designed with their help [3, 4]. More recently, the development of LES has allowed detailed studies of turbulent combustion. Even though the cost of such LES remains very high, the predictive capacities of these tools for turbulent combustion have been clearly demonstrated [3, 4]. Extending LES to study flame/acoustics coupling is therefore an obvious research path [5, 6]. The experimental conguration is described first before providing short descriptions of the LES. Some results are described for the combustor reacting case at equivalence ratio 0.7.

1.1 Configuration

The studied conguration is the so-called PRECCINSTA burner, experimentally investigated by Meier et al. [1]. Its focus is the validation of Large-Eddy Simulation models in realistic conditions. This geometry has been widely used as a validation database for combustion models or for numerical methods applied to the solving of the NavierStokes equations. The experimental conguration is described first before providing short descriptions of the LES tools. The gas turbine model combustor was derived from an industrial design by Turbomeca. In Fig.1.1 a schematic of the nozzle design with the combustion chamber is shown.

Dry air at ambient temperature is fed via a plenum (ϕ = 78 mm) through 12 radial swirler vanes to the burner nozzle. The fuel gas (CH_4) is injected into the air flow through small holes (ϕ = 1 mm) within the radial swirler with high momentum to ensure good mixing before it enters the combustion chamber. The nozzle exit has a diameter of 27.85 mm. The combustion chamber consists of large quartz windows of thickness 1.5mm held by steel posts in the corners, thus creating a connement with a square section of 85x85 mm and a height of h = 114mm. The exit of the upright combustion chamber is cone shaped, leading to a short central exhaust pipe with a diameter of 40 mm. For these operating conditions the Reynolds number at the exit of the nozzle, based on the cold flow and the exit diameter, is about 35000 and the swirl number, derived from the velocity measurements at 1.5mm above the exit, is approximately 0.6.

Fig.1.2 shows slices at x = 0 and z = −0.03 cm with grid adopted in the simulation with the HeaRT code. In the same figure the shade of the burner geometry is also shown. The grid consists of ∼ 53000000 grid points with 320x320x512 nodes in the x-y-z directions respectively. The not-unifrom grid is refined near CH_4 injection holes and near the exit of the central conical hub. The burner operates at atmospheric pressure and the inlet air temperature is 300 K. At the inlet of the plenum, a flat 24.5 ms^{-1} velocity profile is imposed and it was checked that this profile had no influence on the results as long as the total mass-flow rate was conserved.

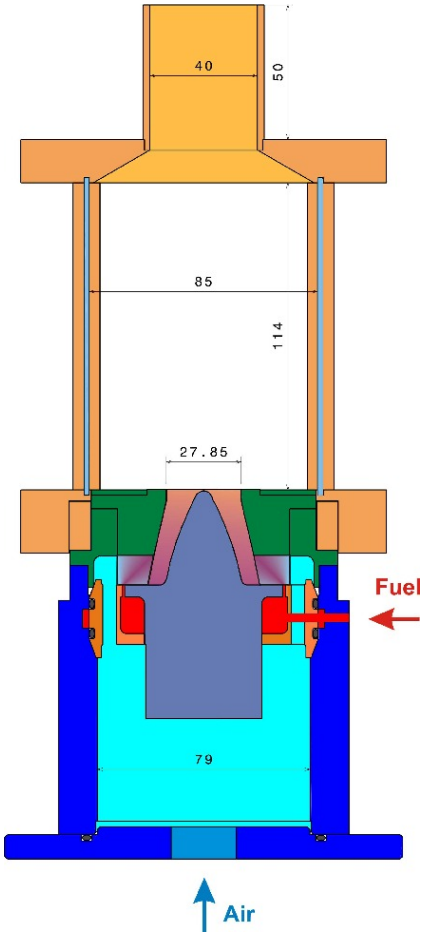

Figura 1.1: Schematic of the injectors, swirler and combustion chamber.

1.2 Governing Equations

In LES each turbulent field variable is decomposed into a resolved and a subgrid-scale part. In this work, the spatial filtering operation is implicitly defined by the local grid cell size. Variables per unit volume are treated using Reynolds decomposition, while Favre (density weighted) decomposition is used to describe quantities per mass unit. The instantaneous small-scale fluctuations are removed by the filter, but their statistical effects remain inside the unclosed terms representing the influence of the subgrid scales on the resolved ones. In this article, a test deals with combustion to show the robustness of the suggested technique. Gaseous combustion is governed by a set of transport equations expressing the conservation of mass, momentum and energy, and by a thermodynamic equation of state describing the gas behavior. For a mixture of N_s ideal gases in local thermodynamic equilibrium but chemical non-equilibrium, the corresponding filtered field equations (extended Navier−Stokes equations) are:

- Transport Equation of Mass

$$\frac{\partial \overline{\rho}}{\partial t} + \frac{\partial \overline{\rho} \widetilde{u_i}}{\partial x_i} = 0, \tag{1.1}$$

- Transport Equation of Momentum

$$\frac{\partial (\overline{\rho} \widetilde{u_j})}{\partial t} + \frac{\partial (\overline{\rho} \widetilde{u_i} \widetilde{u_j} + \overline{p} \delta_{ij})}{\partial x_i} = \frac{\partial \widetilde{\tau}_{ij}}{\partial x_i} + \frac{\partial \tau_{ij}^{sgs}}{\partial x_i}, \tag{1.2}$$

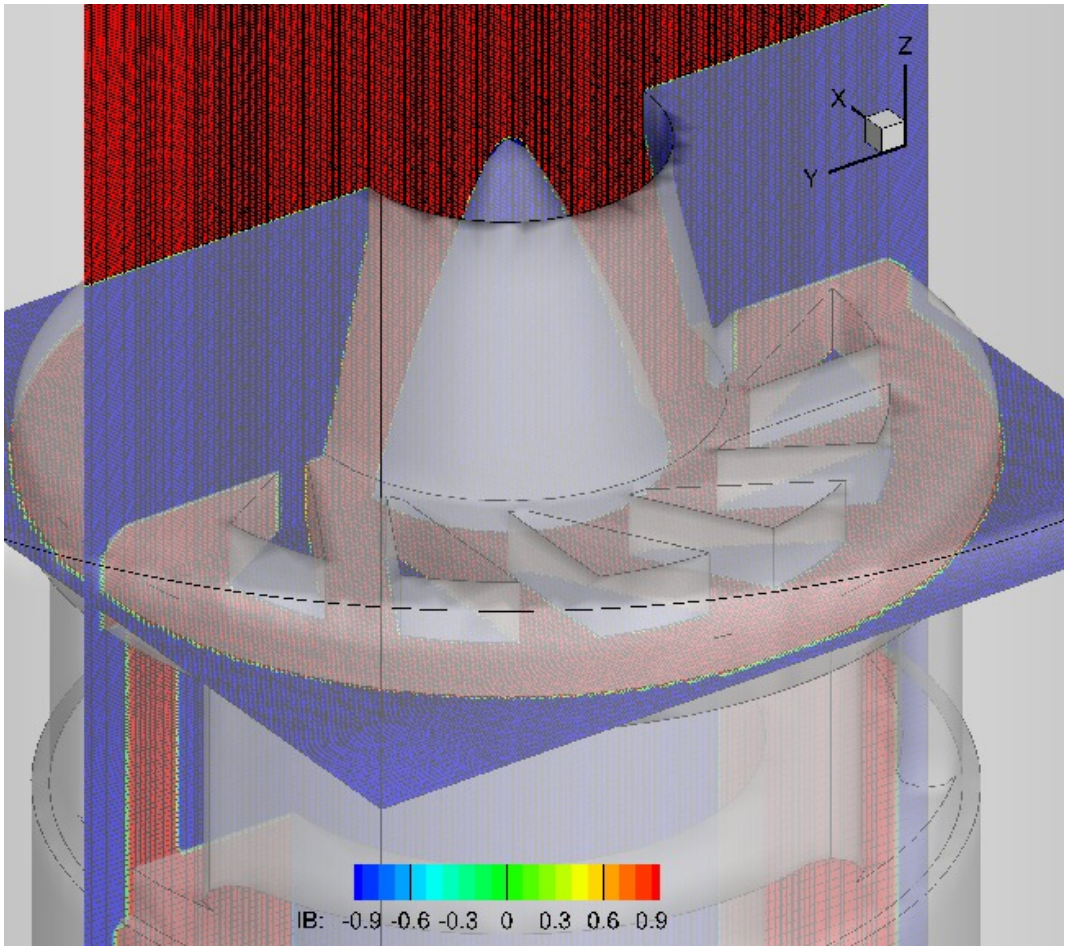

Figura 1.2: Computational grid used for the simulation in the HeaRT code. Slices of plane at x = 0 cm and z = −0.03 cm, coloured by IVM factor IB (IB = 1 in fluid region and IB = −1 inside the solid geometry).

- Transport Equation of Total Energy (internal + mechanical, $\mathcal{E} + \mathcal{K}$)

$$\frac{\partial(\overline{\rho}\,\widetilde{\mathcal{U}})}{\partial t} + \frac{\partial(\overline{\rho u_i}\widetilde{\mathcal{U}} + \overline{p u_i})}{\partial x_i} = -\frac{\partial(\overline{q_i} - \widetilde{u}_j\overline{\tau_{ij}} + H_i^{sgs} + q_i^{sgs})}{\partial x_i}, \tag{1.3}$$

- Transport Equation of the N_s Species Mass Fractions

$$\frac{\partial(\overline{\rho}\,\widetilde{Y}_n)}{\partial t} + \frac{\partial(\overline{\rho u}_j\widetilde{Y}_n)}{\partial x_i} = -\frac{\partial}{\partial x_i}(\widetilde{J}_{n,i} + \widetilde{J}_{n,i}^{sgs}) + \widetilde{\dot{\omega}}_n, \tag{1.4}$$

- Thermodynamic Equation of State

$$\overline{p} = \overline{\rho}\sum_{n=1}^{N_s}\frac{\widetilde{Y}_n}{W_n}\mathcal{R}_u\widetilde{T}. \tag{1.5}$$

These equations must be coupled with the constitutive equations which describe the molecular transport. In the above equations, t is the time variable, ρ the density, u_j the velocities, τ_{ij} the viscous stress tensor, $\widetilde{\mathcal{U}}$ the total filtered energy per unit of mass, that is the sum of the filtered internal energy, $\widetilde{e}$, and the resolved kinetic energy, $1/2\,\widetilde{u_i}\widetilde{u_i}$, q_i is the heat flux, p the pressure, T the temperature, $\mathcal{R}_u$ is the universal gas constant, W_n the

nth-species molecular weight, $\dot{\omega}_n$ is the production/destruction rate of species n, diffusing at velocity $V_{i,n}$ and resulting in a diffusive mass flux $\boldsymbol{J_n} = \rho Y_n \boldsymbol{V_n}$. The stress tensor and the heat flux are respectively:

$$\overline{\tau_{ij}} = 2\mu\,(\widetilde{S_{ij}} - \frac{1}{3}\widetilde{S_{kk}}\delta_{ij}), \tag{1.6}$$

$$\overline{q_i} = -k\frac{\partial \widetilde{T}}{\partial x_i} + \overline{\rho}\sum_{n=1}^{N_s}\widetilde{h_n}\widetilde{Y_n}\widetilde{V_{i,n}}. \tag{1.7}$$

In this equations μ is the molecular viscosity and k is the thermal conductivity. Kinetic theory is used to calculate dynamic viscosity and thermal conductivity of individual species [13]. The mixture-average properties are estimated by means of Wilke's formula with Bird's correction for viscosity [14, 15], and Mathur's expression for thermal conductivity [16].

Eqn. 1.7, the first term is the heat transfer by conduction, modeled by Fourier's law, the second is the heat transport due to molecular diffusion acting in multicomponent mixtures and driven by concentration gradients. The Hirschfelder and Curtiss approximate formula for mass diffusion $\boldsymbol{V_n}$ in a multicomponent mixture is adopted, i.e.,

$$\boldsymbol{J_n} = \rho Y_n \boldsymbol{V_n} = -\rho Y_n D_n \frac{\nabla X_n}{X_n} = -\rho \frac{W_n}{W_{mix}} D_n \nabla X_n\ , \tag{1.8}$$

where $X_n = Y_n W_{mix}/W_n$ and the D_n is

$$D_n = \frac{1 - Y_n}{\sum_{j=1,\ j\neq n}^{N_s} \frac{X_j}{\mathcal{D}_{jn}}}\ . \tag{1.9}$$

$\mathcal{D}_{jn}$ being the binary diffusion coefficient. When inexact expressions for diffusion velocities are used (as when using Hirschfelder's law), and in general when differential diffusion effects are considered, the constrain $\sum_{i=1}^{N_s}\boldsymbol{J_i} = \sum_{i=1}^{N_s}\rho Y_i \boldsymbol{V_i} = 0$ is not necessarily satisfied. In this paper, to impose mass conservation, an artificial diffusion velocity $\boldsymbol{V^c}$ is subtracted from the flow velocity in the species transport equations [5]. This velocity, assuming Hirschfelder's law holds, becomes:

$$\boldsymbol{V^c} = -\sum_{n=1}^{N_s}\frac{W_n}{W_{mix}} D_n \nabla X_n\ . \tag{1.10}$$

In Eqn. 1.2, the subgrid stress tensor, τ_{ij}^{sgs}, is expressed through a Smagorinsky model:

$$\tau_{ij}^{sgs} = -\overline{\rho}(\widetilde{u_i u_j} - \widetilde{u_i}\widetilde{u_j}) \simeq 2C_R(\boldsymbol{x}, t)\overline{\rho}\Delta^2\Pi^{\frac{1}{2}}(\widetilde{S}_{ij} - \frac{1}{3}\overline{\rho}q^2\delta_{ij}), \tag{1.11}$$

where $1/3\,\overline{\rho}q^2$ is the subgrid kinetic energy, $\widetilde{S}_{ij} = 1/2\left(\partial\widetilde{u_i}/\partial x_j + \partial\widetilde{u_j}/\partial x_i\right)$ is the filtered strain rate tensor, $\Pi^{1/2} = \sqrt{2\widetilde{S}_{ij}\widetilde{S}_{ij}}$ is its module, $\Delta = \sqrt[3]{Volume}$ is the grid filter width, and C_R is the constant of the subgrid stress model, here dynamically computed. The unclosed subgrid reaction rates in the Eqn. (1.4), are modeled using the Fractal Model FM, details of which can be found in previous works [12]. In Eqn. 1.3, the subgrid energy flux H^{sgs} is modelled as $\mu_t/Pr_t\frac{\partial\widetilde{H}}{\partial x_i}$, Pr_t being the turbulent Prandtl number here assumed 0.9, while the subgrid heat transfer q_i^{sgs} as $-(\mu_t + \mu_l)\mu_t/k\,\partial\widetilde{T}/\partial x_i$.

In the transport equation of the N_s Species Mass Fraction (Eqn. 1.4), the subgrid mass flux $\widetilde{J}_{n,i}^{sgs}$ is modelled using a gradient assumption as $\mu_t/Sc_t\partial\widetilde{Y_n}/\partial x_i$, Sc_t being the turbulent Schmidt number, here assumed 0.7.

The finite difference code is second-order accurate. In the case of premixed reactive flows the convective species and energy fluxes are computed adopting a third-order modified version of the advection upstream splitting method (AUSM) to reduce spurious oscillations due to strong unresolved density gradients in the flame front. Time-integration of Navier-Stokes equations (1.1-1.4) is performed by means of the fully explicit third-order accurate TVD Runge-Kutta scheme of Shu and Osher [20].

2 Numerical Results

2.1 Results and discussion

Figure 2.1 shows a 3D view of the $c = 0.6$ progress variable iso-surface. The flame has a V-shape with an anchoring on the head and the corners of the swirler. The wrinkling of the flame seems higher in the downstream locations with smaller structures. In Fig. 2.1, also it is shown the isosurface of methane mass fraction $Y_{CH_4} = 0.1$ coloured by axial velocity, at the jet fuel inlet the velocity is approximately $U_z = 70\,\mathrm{ms}^{-1}$.

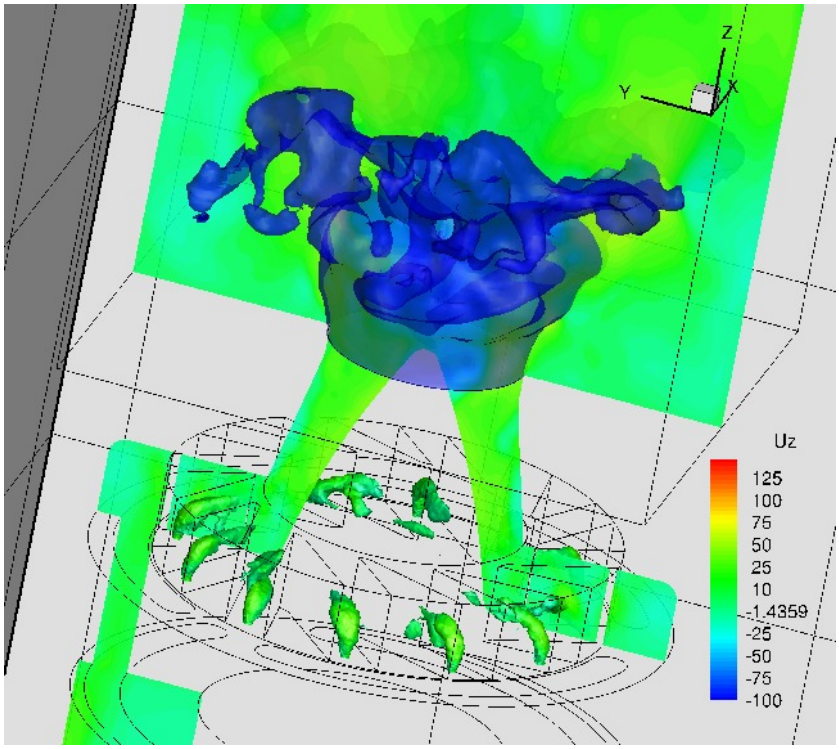

Figura 2.1: Iso-contour c = 0.6 of progress variable and of $Y_{CH_4} = 0.12$ coloured by axial velocity U_z. Instantaneous snapshot of axial velocity U_z.

Figure 2.2 shows slice at y = 0 of mean axial velocity U_z and two isosurface of axial velocities at $25\mathrm{ms}^{-1}$ (in green) and $-10\mathrm{ms}^{-1}$ (in blue). Inside the combustion chamber it is possible to identify two recirculation zones. The first one is centered near the z simmetry axis and it is due to the swirled inlet profile. In fact, once the flow enter in the combustion chamber, it rapidly reach the vertical lateral wall, creating a pressure decrease at the exit of the swirler near the z axis, this pressure decrease recalls flow from the lateral zone of the combustion chamber and it creates this elliptic recirculation zone with a minimum axial velocity of $U_z = -25\,\mathrm{ms}^{-1}$ (indicated in Fig 2.2 with R1), promoting the stabilization of the flame at the exit of the swirler. The second recirculation zone has a toroidal shape and it extends laterally between the exit flow stream and the wall of the combustion chamber (indicated in Fig 2.2 with R2). This outer recirculation zone is characterized by very low axial velocities and radial velocities that are directed to the flame axis. The maximum mean axial velocity is reached at the exit of the combustion chamber near the cylindrical outlet pipe.

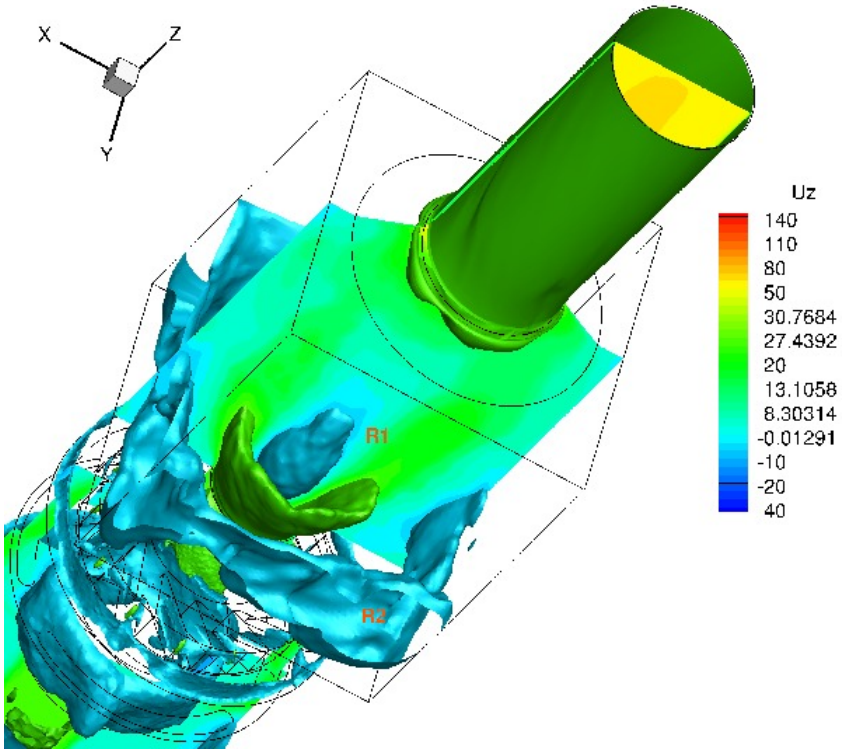

Figura 2.2: Slice of mean axial velocity profile at y = 0, isosurface of axial velocity $U_z = 25 ms^{-1}$ and $U_z = -10 ms^{-1}$

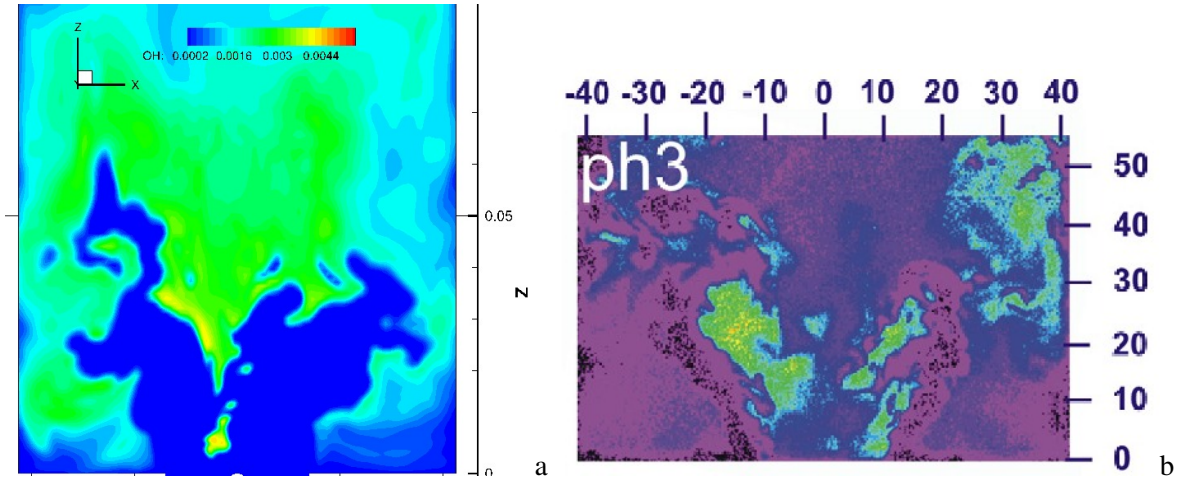

Figura 2.3: Instantaneous OH mass fraction profile at y = 0. a)Numerical; b)Experimental single-shot OH PLIF image. Scales at axes are in mm; color bar is given in arbitrary units.

Figure 2.3a-b shows instantaneous OH mass fraction at $y = 0$ plane from numerical simulation and experiment. At chemical equilibrium, the OH concentration increases exponentially with temperature. The increase is, however, different for fuel lean and fuel-rich mixtures. In fuel-lean mixtures, OH concentrations are detectable above $T \sim 1400 - 1500K$. In reaction zones, OH is formed in superequilibrium concentrations, which in turbulent flames are typically several times higher than at equilibrium. The lifetime of this superequilibrium

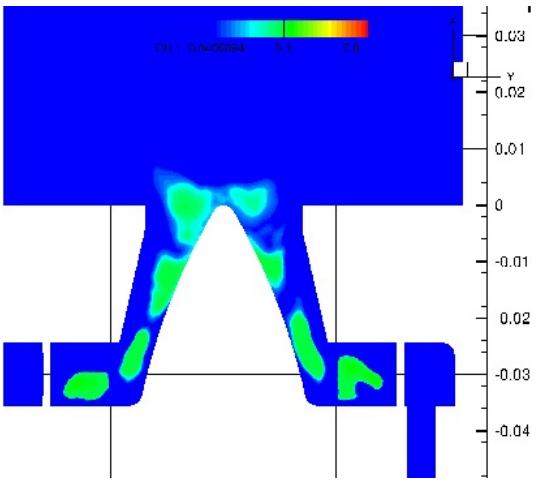

Figura 2.4: Mean profile of CH_4 at the conical hub exit.

OH is several milliseconds at atmospheric pressure. Thus, the highest OH concentrations within a PLIF image (or numerical snapshot) stem probably from superequilibrium OH, i.e., young OH that has just been formed in a reaction zone. In the image, the region around the flame axis (z > 0.05cm) shows medium OH intensities (green color) which most probably reflect old OH at rather high temperatures. On each side of this region there are high OH mass fraction intensities (yellow) from z = 0.01 to 0.03cm. These stem presumably from young OH, i.e., from the reaction zones. In the outer recirculation zones (R2 in Fig. 2.2) the OH mass fractions are quite low, reflecting old OH at intermediate temperatures. Although CH_4 and Air are mixed in the swirler ducts, by injecting methane at high velocity, a sigificant level of unmixedness was revealed at the exit of the conical hub. This is shown in detail in Fig. 2.4 where the available mean CH_4 mass fraction at y = 0. In the time simulated, the mixture exit section (z = 0m) don't present a uniform value of the fuel mass fraction, since the CH_4 lies close to the surface of the conical hub.

2.2 Conclusions

A gas turbine burner for premixed flames ($\phi = 0.7$) has been studied with Large Eddy Simulation (LES). The flow field could be divided into three different regimes: the inflow of fresh gases and an inner and an outer recirculation zone. The flames were anchored below the nozzle exit plane close to the inner recirculation zone, but the main flame zone appeared at ~ 0.035 m. A significant level of unmixedness was revealed at the exit of the conical hub (see Fig. 2.4). This suggest, with these partial results, that some instabilities may occur in the flame due to the not perfect level of mixing. Since a very fine grid and a kinetic scheme with 17 species was adopted in the simulation of this combustor with an homemade code (in leterature we found LES with reduced kinetic schemes [4], Direct numerical Simulation with tabulated chemistry [3] and LES with detailed chemistry using Fluent [22]), the costs of numerical simulation is very high and a full statistic of the simulation is not yet reached, as it is possible to see from the mean profile of axial velocity and fuel mass fraction. The simulation is running and in the next year a complete set of data will be available for the comparison of numerical results with experiments.

Bibliografia

[1] W. Meier, P. Weigand, X. Duan, R. Giezendanner-Thoben, Combust. Flame 150 (1-2) (2007) 2-26.

[2] D. Cecere, E. Giacomazzi, An Immersed Volume Method for Large Eddy Simulation of Compressible Flows using a Staggered-Grid Approach, Computer Methods App. Mech., 280, (2014), 1-27.

[3] V. Moureau, P. Domingo, L. Vervisch, From Large-Eddy Simulation to Direct Numerical Simulation of a lean premixed swirl ame: Filtered laminar ame-PDF modeling,158,(2011), 1340-1357.

[4] S. Roux,G. Lartigue, T. Poinsot, U. Meier, C. Bérat, Studies of mean and unsteady ow in a swirled combustor using experiments, acoustic analysis, and large eddy simulations, Combustion and Flame, 141, (2005) 40-54.

[5] T. Poinsot, D. Vaynante, Theoretical and numerical combustion, 2012.

[6] H. Forkel, J. Janicka, Flow Turb. Combust. 65 (2000) 163-175.

[7] E.R. Hawkes, J.H. Chen, Direct numerical simulation of hydrogen-enriched lean premixed Methane-Air Flames, Combust. Flame 138 (2004) 242-58.

[8] R. Sankaran, E.R. Hawkes, J.H. Chen, T. Lu, C.K. Law, Structure of a spatially developing turbulent lean methane-air Bunsen flame, Proc. Combust. Inst., 31, (2007) 1291-1298.

[9] M. Klein, A. Sadiki, J. Janicka, A digital filter based generation of inflow data for spatially developing direct numerical or large eddy simulations, J. Comput. Phys. 186, (2003), 652-665.

[10] T.J. Poinsot, S.K. Lele: Boundary Conditions for Direct Simulations of Compressible Viscous Flow. J. Comput. Phys., 101:104-129 (1992).

[11] J.C. Sutherland , C.A. Kennedy , Improved boundary conditions for viscous, reacting, compressible Flows, J. Comput. Phys., 191:502-524, 2003

[12] E. Giacomazzi, V. Battaglia and C. Bruno, The Coupling of Turbulence and Chemistry in a Premixed Bluff-Body Flame as Studied by LES, Combust. Flame, 138 (2004) 320-335.

[13] R.B. Bird, W.E. Stewart, E.N. Lightfoot, Transport Phenomena, Wiley International Edition, (2002).

[14] C.R. Wilke, J. Chem. Phys., 18, (1950), 517-9.

[15] R.J. Kee, G. Dixon-Lewis, J. Warnatz, M.E. Coltrin, Miller JA, Moffat HK, The CHEMKIN Collection III: Transport, San Diego, Reaction Design, (1998).

[16] S. Mathur, P.K. Tondon, S.C.Saxena, Molecular Physics, 12:569, (1967).

[17] J.H. Ferziger, H.G. Kaper, Mathematical Theory of Transport Processes in Gases, North Holland Pub. Co., Amsterdam, 1972.

[18] W.H. Furry, Am. J. Phys. 16 (1948) 63-78.

[19] E. Giacomazzi, F.R. Picchia, N.M. Arcidiacono, A Review on Chemical Diffusion, Criticism and Limits of Simplified Methods for Diffusion Coefficients Calculation, Combust. Theory Model., (2008).

[20] C.W. Shu, S. Osher, Efficient implementation of essentially non-oscillatory shock-capturing schemes, J. Comput. Phys., 77, 439-471 (1988).

[21] M.S. Mansour, N. Peters, Y.C. Chen, Proc. Combust. Inst. 27 (1998) 767-773.

[22] A. Di Nardo, G. Calchetti, S. Chiocchini, E. Giacomazzi, E. Giulietti, LARGE EDDY SIMULATION OF A PULSATING PREMIXED FLAME, XXXVI Meeting of the Italian Section of the Combustion Institute, (2013).